Air-Coupled Through-Transmission Fan-Beam Tomography Using Divergent Capacitive Ultrasonic Transducers

William M. D. Wright, *Member, IEEE*, Paul Ingleby, and Ian J. O'Sullivan

***Abstract*—A pair of divergent air-coupled capacitive ultrasonic transducers (CUTs) with curved backplates was used to acquire signals through regions of air containing solid objects, air flow, and temperature fields. Fan-beam datasets were collected and used in a tomographic reconstruction algorithm to produce cross-sectional images of the area under interrogation. In the case of the solid objects, occluded rays from the projections were accounted for using a compensation algorithm and a priori knowledge of the object. A rebinning routine was used to pick out parallel ray sets from the fan-beam data. The effects of further reducing the number of datasets also were investigated, and, in the case of imaging solid objects, characteristic Gibbs phenomena were seen in the reconstructions as expected. However, when imaging temperature and flow fields, the aliasing artefacts were not seen, but the reconstructed values decreased with the size of dataset used. The effect of changing the kernel filter function also was investigated, with the different filters giving the best compromise between image noise, reconstruction accuracy, and amount of data required in each scenario.**

I. Introduction

Ultrasonic tomographic imaging is receiving much interest at present as a noninvasive, nondestructive evaluation (NDE) technique for visualizing the internal structure or spatial variations in properties of a number of different media. Although a well-established technique in medicine [1] and geophysics [2], the many various tomographic reconstruction methods [3]–[9] have received relatively little attention in engineering. Previously reported uses of ultrasonic tomography have included flow and process engineering applications [10], [11], NDE of trees [12], and solid propellant rocket motors [13] using bulk waves, and other applications using Lamb waves [14], [15]. Scant attention has been paid to ultrasonic tomography in gaseous media. Until recently, the primary limitation of this application of the technique had been the lack of suitable air-coupled ultrasonic transducers. With advances in capacitive [16], [17], piezopolymer [18], piezocomposite [19], and capacitive micromachined ultrasonic transducer (cMUT) [20]–[23] devices that all operate efficiently in air, work has been carried out that has investigated the location of solid objects in air [24], temperature and flow fields in gases [25], and imaging of gas jets and flames [26], [27].

In the majority of the cited works, the reconstruction algorithm used was based on a parallel-beam geometry using the Fourier slice technique [3]. This method requires the collection of a number of parallel rays through the region of interest at a particular angle, then either the transducers or the test subject are rotated, and the process is repeated until a full 180° or 360° dataset has been acquired. This usually results in a large quantity of data and long acquisition times; depending on the reconstruction technique, the resolution of the images usually is determined by the spatial sampling rate, the spatial Nyquist limit, and the ultrasonic frequency.

A more efficient sampling geometry is to use a fan-beam configuration, in which rays emanating from a single divergent source are propagated through the imaging plane over a range of different angles simultaneously to an array of receivers that is spaced equally in either angle or distance. This work will demonstrate that equivalent images to earlier work using parallel beams [25] can be obtained with reduced datasets acquired using a fan-beam geometry, and it is a logical progression of this earlier study. The effects of aliasing on the images produced also will be investigated when the size of the dataset is further reduced, as will the effects of windowing the kernel function used in the filtered back-projection algorithm.

Locating solid objects in gaseous media, and imaging of the properties of the gaseous media itself, are usually mutually exclusive tomographic events. Previous work [24] has simply located the object in the imaging plane and paid little attention to the properties of the surrounding air. Any solid object effectively occludes certain rays in the reconstruction. In this work, the occluded data was compensated for using an algorithm that required some basic a priori knowledge of the gaseous media and solid object. Assuming the object dimensions and the speeds of sound in the gas and solid were known, artificial propagation delay data was calculated based on the relative lengths of the ray path in the solid and gas, respectively. This artificial data then was substituted for the occluded rays. Although internal features within the solid could not be reconstructed, this technique minimized the effects of the occluded data on the rest of the image and allowed more

Manuscript received December 27, 2004; accepted June 10, 2005. P. I. was supported during this work by a Marie-Curie Individual Fellowship (Category 30), contract number HPMF-CT-1999-00038.

W. M. D. Wright and I. J. O'Sullivan are with the Department of Electrical and Electronic Engineering, University College Cork, National University of Ireland - Cork College Road, Cork, Ireland (e-mail: Bill.wright@ucc.ie).

P. Ingleby is with SELEX Sensors and Airborne Systems, Crewe Toll, Edinburgh, UK.

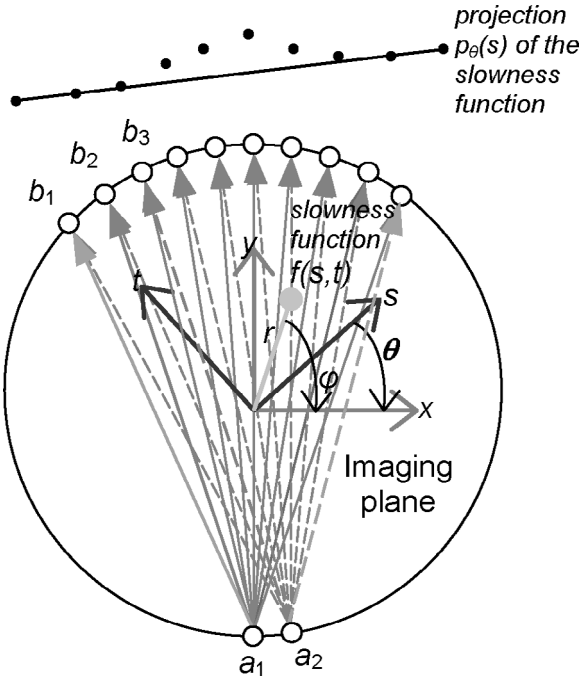

Fig. 1. Tomographic fan-beam scan geometry.

accurate reconstruction of the properties of the surrounding gaseous media. Thus, the same through-transmission reconstruction algorithm could be used to simultaneously reconstruct the solid object distribution and the gas properties within the imaging plane.

II. Divergent Air-Coupled Capacitive Ultrasonic Transducers

Consider the tomographic fan-beam sampling geometry shown schematically in Fig. 1. A single transmitter a and an array of receivers b produce a fan-shaped dataset of ultrasonic rays that pass through the imaging plane at regular angular intervals. The transmitter position then is rotated by $\Delta\theta$, and the procedure is repeated. It can be seen in Fig. 1 that ray a_1b_2 from the first fan is parallel to ray a_2b_3 in the second fan, and so on. From a set of fans covering 180° or a full 360°, a full set of parallel beams at each angle θ may be picked out in a process known as rebinning [28]. These parallel ray sets then may be used in a parallel-beam reconstruction algorithm provided that the rays are scaled to be of uniform length, and the rays are interpolated to be equidistant. The length L_n of each ray is extended by extrapolating by δL_n as required, assuming that the acoustic slowness along the raypath outside the scan area is identical to the background slowness value within the scanned region, increasing the total propagation time from t_n to T_n for each ray according to:

$$T_n = \left(\frac{2\delta L_n}{c_{ref}}\right) + t_n, \tag{1}$$

where c_{ref} is obtained from the first ray (L_0, t_0). The rebinned projections then may be used in a standard parallel beam filtered back projection reconstruction algorithm. This procedure has been adequately documented elsewhere [29]. By measuring the propagation delays across the region of interest, images of slowness variations may be produced that then may be related to objects, temperatures, and flow fields in the scanning plane.

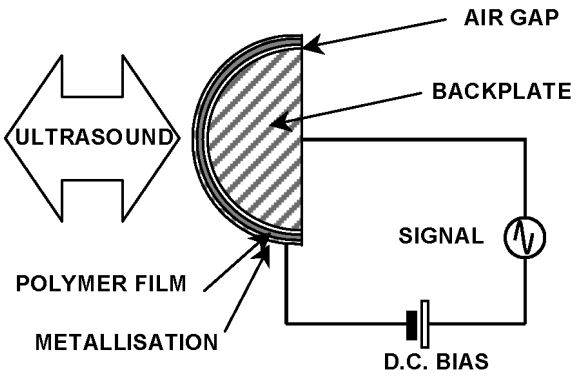

(a)

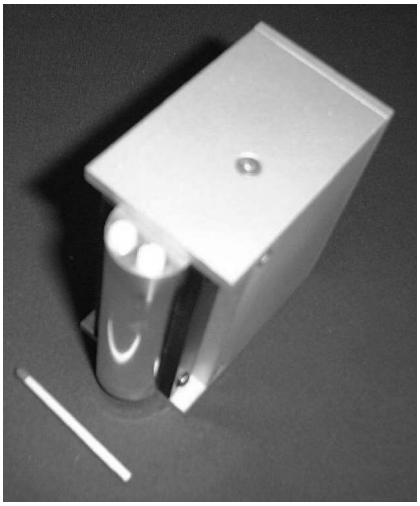

(b)

Fig. 2. (a) Schematic of a divergent capacitive air-coupled transducer. (b) Photograph of a constructed divergent CUT device.

It can be seen from Fig. 1 that, in order to maximize the coverage of each fan, and hence the radius of the reconstruction, divergent transducers producing a wide-angle beam are required. With piezocomposite and cMUT technologies, this type of device is difficult to manufacture; however, it is relatively straightforward using conventional air-coupled capacitive ultrasonic transducers (CUTs) with a flexible polymer electrode and a curved backplate. Such a device was designed for the current study and is shown schematically in Fig. 2(a), with a photograph of a typical device shown in Fig. 2(b). The device consisted of a 5-μm PET membrane metallized with aluminium, and a semicylindrical aluminium backplate 10 mm in diameter and 44 mm long. Note the curvature of the device, shown clearly by the reflection of the matchstick in the aluminium coating on the polymer film in Fig. 2(b). A typical response measured between two such devices across 90 mm of still air is shown in Fig. 3(a), with the corresponding frequency

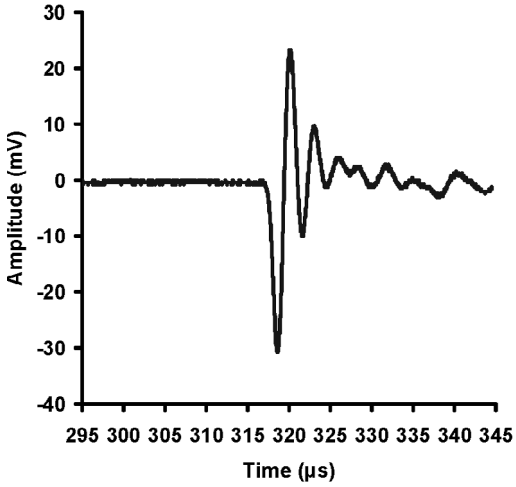

(a)

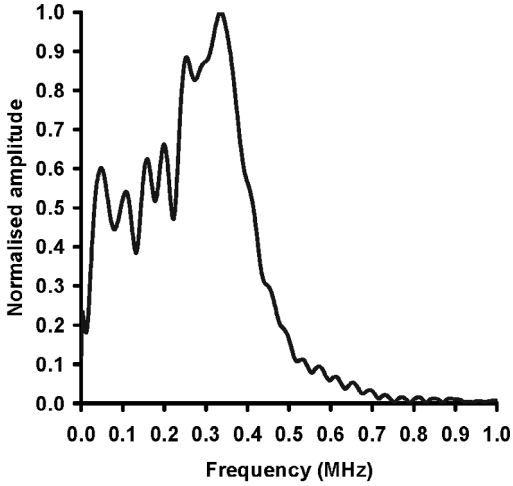

(b)

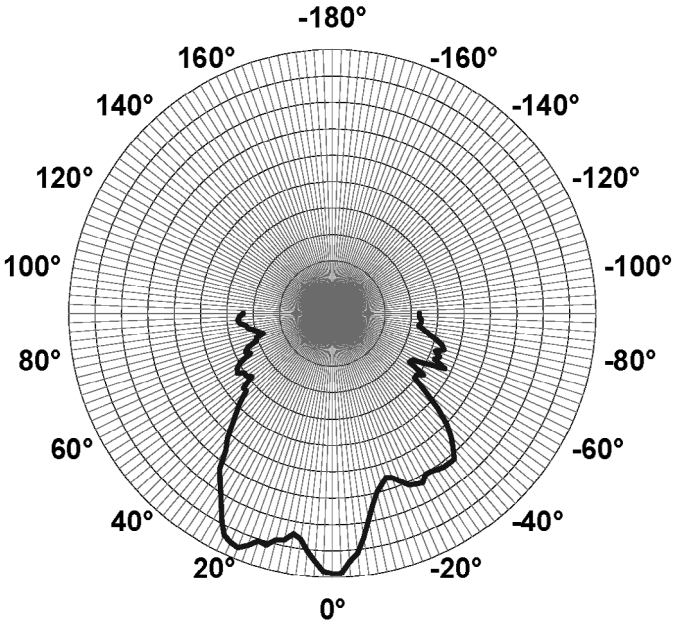

(c)

Fig. 3. (a) Typical time domain waveform across 90 mm of still air. (b) Corresponding frequency spectrum. (c) A directivity plot of the divergent source.

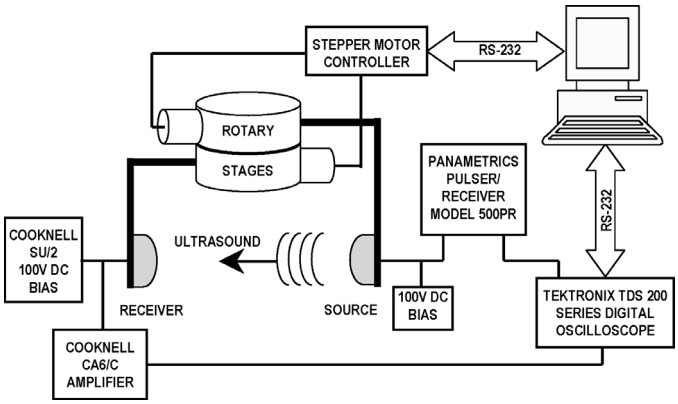

Fig. 4. Schematic of the apparatus used for data acquisition.

spectrum shown in Fig. 3(b), indicating a central frequency of 350 kHz, and a −6 dB bandwidth of 200 kHz. Fig. 3(c) shows a directivity plot taken at a radius of 90 mm at 1° intervals, demonstrating a useful angular range of well over 90°, which is sufficient for the current study. Note that, in this work, only the propagation delay of each ray is considered to produce images of slowness—signal attenuation or frequency content also may be used to produce images of other acoustic properties.

III. Experimental Procedure

A tomographic data acquisition system to collect fan-beam data was set up as shown schematically in Fig. 4. A pair of the curved divergent capacitive air-coupled transducers described earlier was mounted with a separation of 200 mm on a pair of coaxial Daedal rotary stages (Parker Hannifin Corporation, Irwin, PA) under stepper motor control. The transducers could be positioned with an angular precision of ±0.02°, under computer control via a RS-232 interface. The source transducer was driven by a Model 500PR pulser-receiver (Panametrics Inc., Waltham, MA) that delivered a negative spike of up to −250 V with a pulse energy of up to 19.4 μJ, and biased using a 100 V direct current (DC) supply. The receiver was connected to a SU2/C power supply (Cooknell Electronics Ltd., Weymouth, UK) that provided a DC bias of 100 V, and to a CA6/C charge amplifier (Cooknell Electronics Ltd.) with a sensitivity of 250 mV/pC. The received waveforms then were recorded on a TDS210 60 MHz digitizing oscilloscope (Tektronix Inc., Beaverton, OR) and transferred to a computer via a RS-232 interface for storage and analysis. As the experiments were to demonstrate the feasibility of the technique and the operation of the prototype transducers, the data acquisition time was not a consideration, and it would be dramatically improved with a faster interface. The images also were reconstructed separately from the data acquisition. A suite of custom LabVIEW® (National Instruments Corporation, Austin, TX) programs carried out the transducer positioning, data acquisition, signal processing, and tomographic reconstructions. Propagation times were found using a simple peak detection algorithm

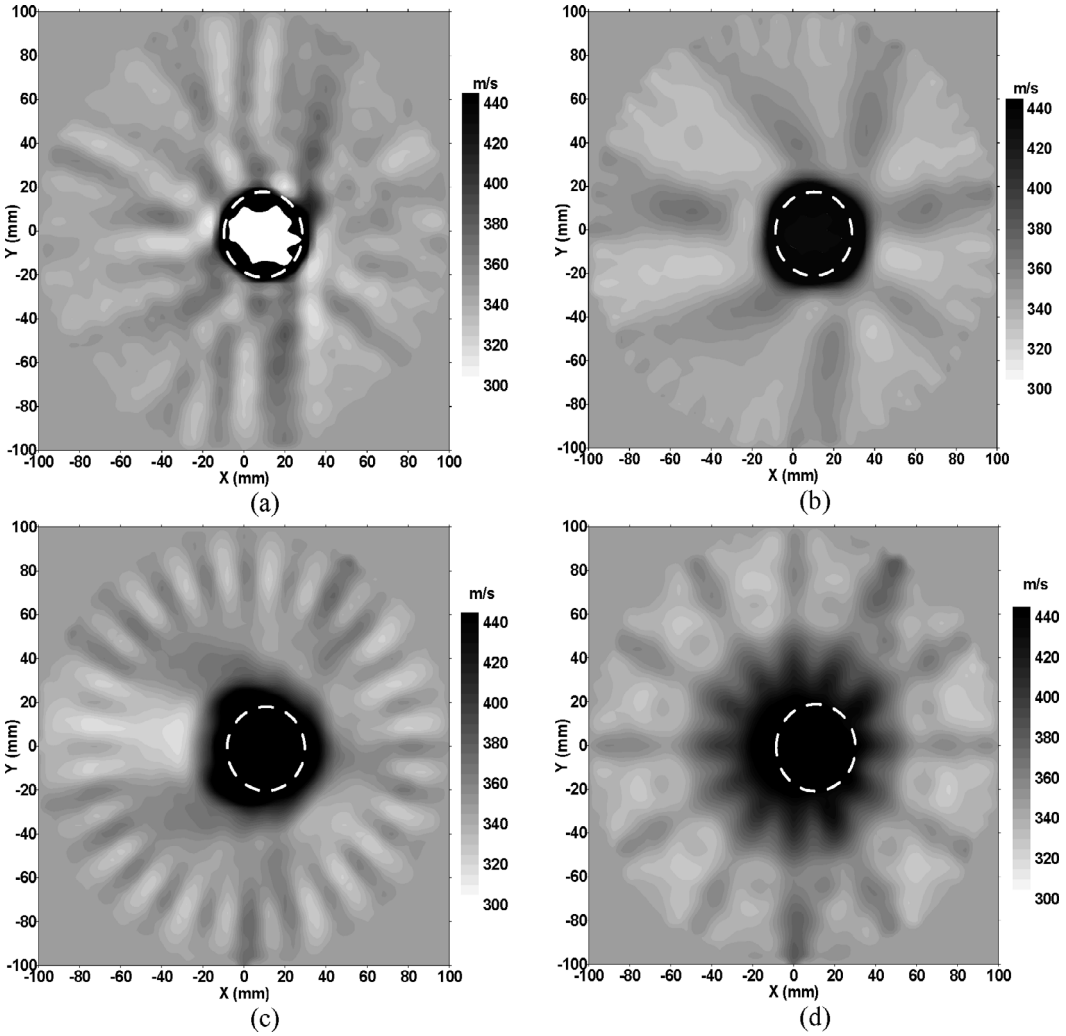

Fig. 5. Images of a 38-mm diameter solid aluminium cylinder in air with its center at (10,0), reconstructed using the Ram-Lak filter. (a) 2664 rays, (b) 684 rays, (c) 312 rays, and (d) 84 rays. The dashed white circle shows the true size and location of the cylinder.

that was sufficient for this study, although more accurate methods such as cross correlation would have improved the results. To collect the fan-beam data, the transmitter position was kept fixed, and the receiver was scanned through a semicircle opposite the transmitter in steps of 5° (i.e., $\Delta\theta$) through 180°, giving a fan-beam of 37 rays. The transmitter and receiver then were rotated together by $\Delta\theta$, and the process was repeated through 360°, giving 72 projections and a total dataset of 2664 rays. In order to simultaneously differentiate between changes in static sound speed due to temperature, and the dynamic velocity changes due to a flow field, opposing rays must be recorded down the same path, as was done in earlier work [25]–[27], [29].

IV. Results and Discussion

A. Simultaneous Reconstruction of Solid Object Distribution and Background Sound Speed

The first series of experiments was to locate solid objects and simultaneously produce images of the speed of sound in the surrounding air, using through-transmission tomographic reconstruction and the occluded data compensation algorithm. An aluminium cylinder of diameter 38 mm was placed with its center at coordinates (0,10) in the scanning plane. The image shown in Fig. 5(a) shows the image reconstructed using 2664 rays (72 projections with 37 rays in each) and a basic Ram-Lak kernel function [3]. The image reproduces the size and location of the cylinder accurately, with the true size and location indicated by the dashed white circle in the image. The irregular white contour in the center of the object is where the reconstructed sound speed is greater than the 440 m/s at the limit of the color scale: this is to be expected as a sound speed of 6320 m/s was used for the occluded ray compensation in the aluminium bar. Despite the large number of occluded rays in each projection, the actual background speed of sound of 343 m/s in the air was reconstructed on average to within 5%. This value was verified from measurements taken without the solid object in place.

It also should be noted that there is a large amount of noise in the image background, due in part to the occluded data and in part to the fast Fourier transforms used

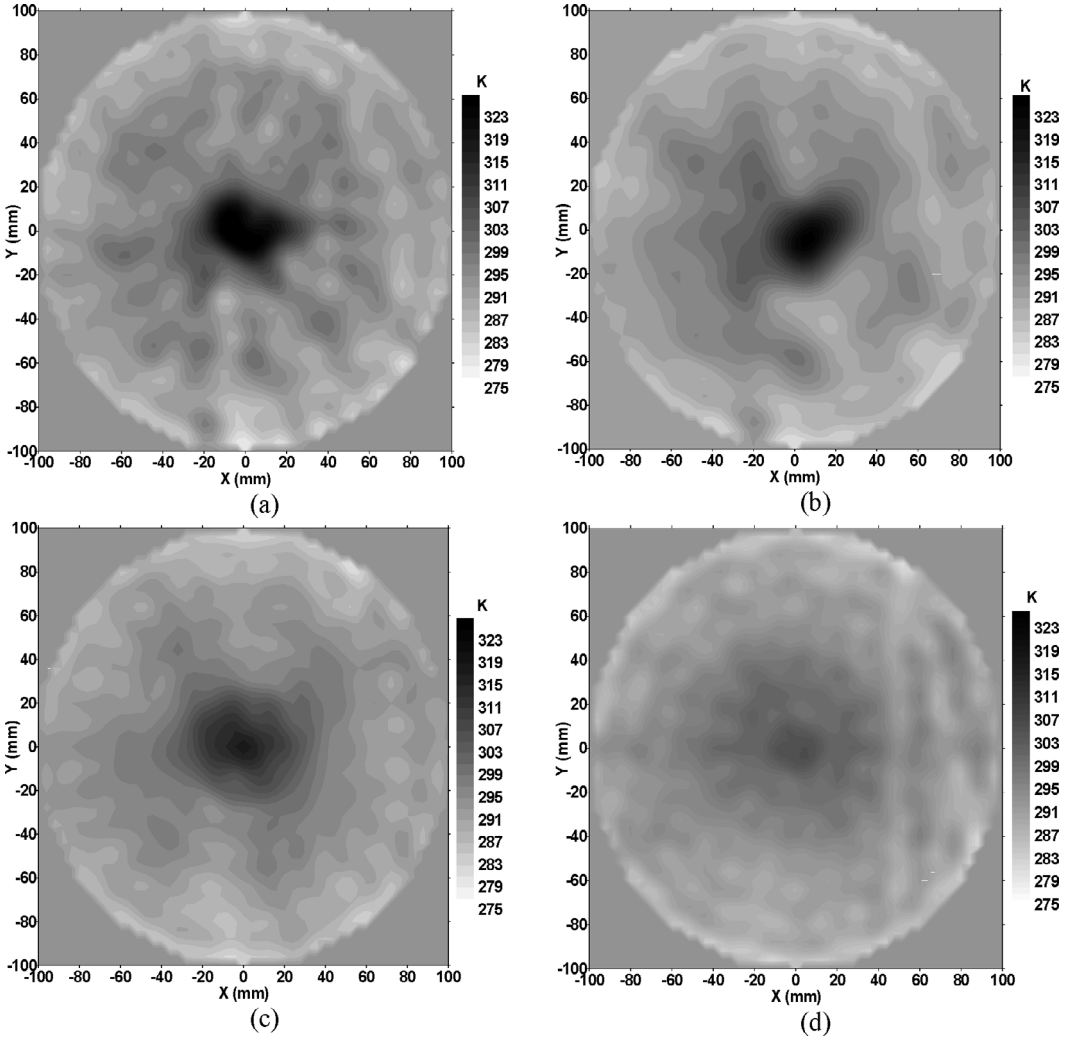

Fig. 6. Reconstructed image of air temperature above a heat source using the Ram-Lak filter. (a) 2664 rays, (b) 684 rays, (c) 312 rays, and (d) 84 rays.

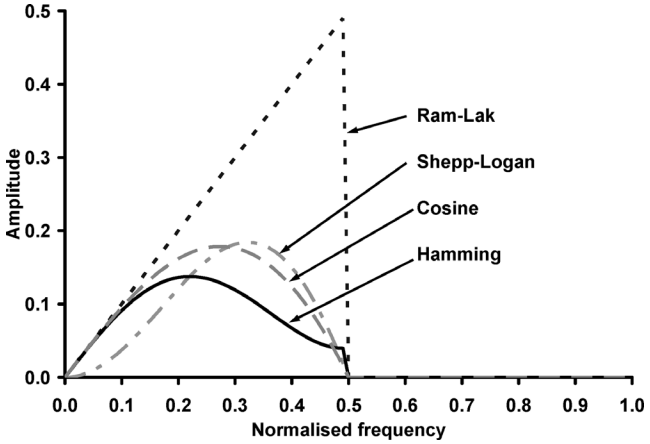

Fig. 7. The different windowed kernel filter functions.

in the reconstruction. As the fan beam from the divergent transmitter was much wider than the solid cylinder, the propagation delay for rays interacting with the edges of the object would be diffracted and scattered, leading to a reduction in amplitude, to the extent that some rays were not accurately recorded. However, propagation delays and not amplitudes were used to reconstruct the images of sound speed. An acoustic penumbra will still be present at the edges of the occluded data region, where the rays are partially obscured and may not be straight lines directly between the source and receivers. This will lead to blurring of the solid boundary and imperfect sizing of the object. Fig. 5(b) shows an image of the same object, but reconstructed using only 684 rays (36 projections with 19 rays in each). The size of the object has not been reproduced as accurately, and there is more noise in the image background. Fig. 5(c) was produced using 312 rays (24 projections with 13 rays in each). It is clear that the size, shape, and position of the object are no longer reconstructed properly. The radial streaks linking the center of the scan area to the transducer positions around the circumference of the image are aliasing defects, and are commonly referred to as Gibbs' phenomena [3]. These are even more pronounced in Fig. 5(d) where only 84 rays were used (12 projections with 7 rays in each), where the reconstruction is clearly putting the object directly in the center of the scanned area. There is insufficient data for

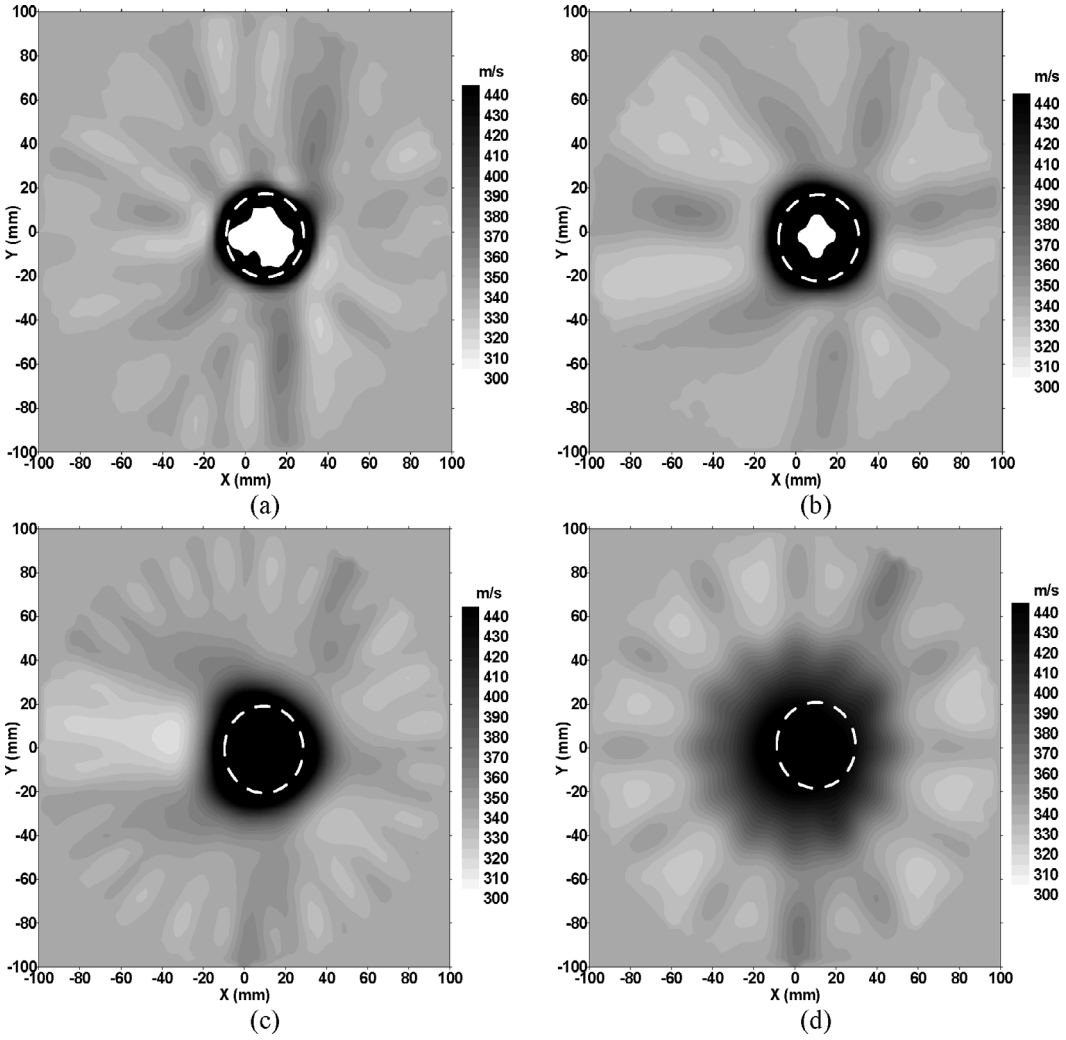

Fig. 8. Images of a 38-mm diameter solid aluminium cylinder in air with its center at (10,0), reconstructed using the cosine filter. (a) 2664 rays, (b) 684 rays, (c) 312 rays, and (d) 84 rays. The dashed white circle shows the true size and location of the cylinder.

the algorithm to resolve the object location. To avoid aliasing when attempting to reconstruct an object of diameter 38 mm, a spatial sampling rate of at least 52.63 samples/m is required. Figs. 5(a) and (b) were sampled at a rate of 122.7 samples/m and 60.25 samples/m, respectively, and show no obvious aliasing effects. Figs. 5(c) and (d) were sampled at a rate of only 39.76 samples/m and 19.23 samples/m, respectively, below the sampling limit.

B. Reconstruction of Air Temperature

For ultrasound propagating in air, the speed of sound c is also related to air temperature T in Kelvin by [30]:

$$c = 331.31\sqrt{\frac{T}{273.16}}. \tag{2}$$

In order to reconstruct a meaningful spatial distribution of air temperature within the scan area, a 6-mm diameter heat source at a constant temperature of 573 K was held close to the center of the scanning area below the scanning plane. The scanning area was surrounded with screens to prevent air currents from disturbing the heated air. Reconstructed slowness values from the fan-beam tomography were converted into temperatures using (2), and the results are shown in Figs. 6(a) to (d) for scans using a Ram-Lak filter and 2664 rays, 684 rays, 312 rays, and 84 rays, respectively. It is clear from Fig. 6(a) that the tomographic algorithms reconstruct a definite heat plume in the correct position within the scan area and that the reconstructed temperatures differ only slightly from those measured with a 1-mm diameter, K-type thermocouple. The room temperature was measured and found to be 294 K, which compared favorably with the tomographic values of between 306 K and 314 K, giving an error in the reconstruction of between 4% and 7%. The reconstructed temperature directly above the heat source was 340 K, but it was measured by the thermocouple to be 344 K, which gives an error of only 1.8%. These fan-beam results compare favorably to earlier parallel-beam work [25].

There are a number of possible reasons for these differences in the temperature measurements. The physical size of the transducers (radius of 10 mm and height of 44 mm) mean that a considerable amount of spatial averaging oc-

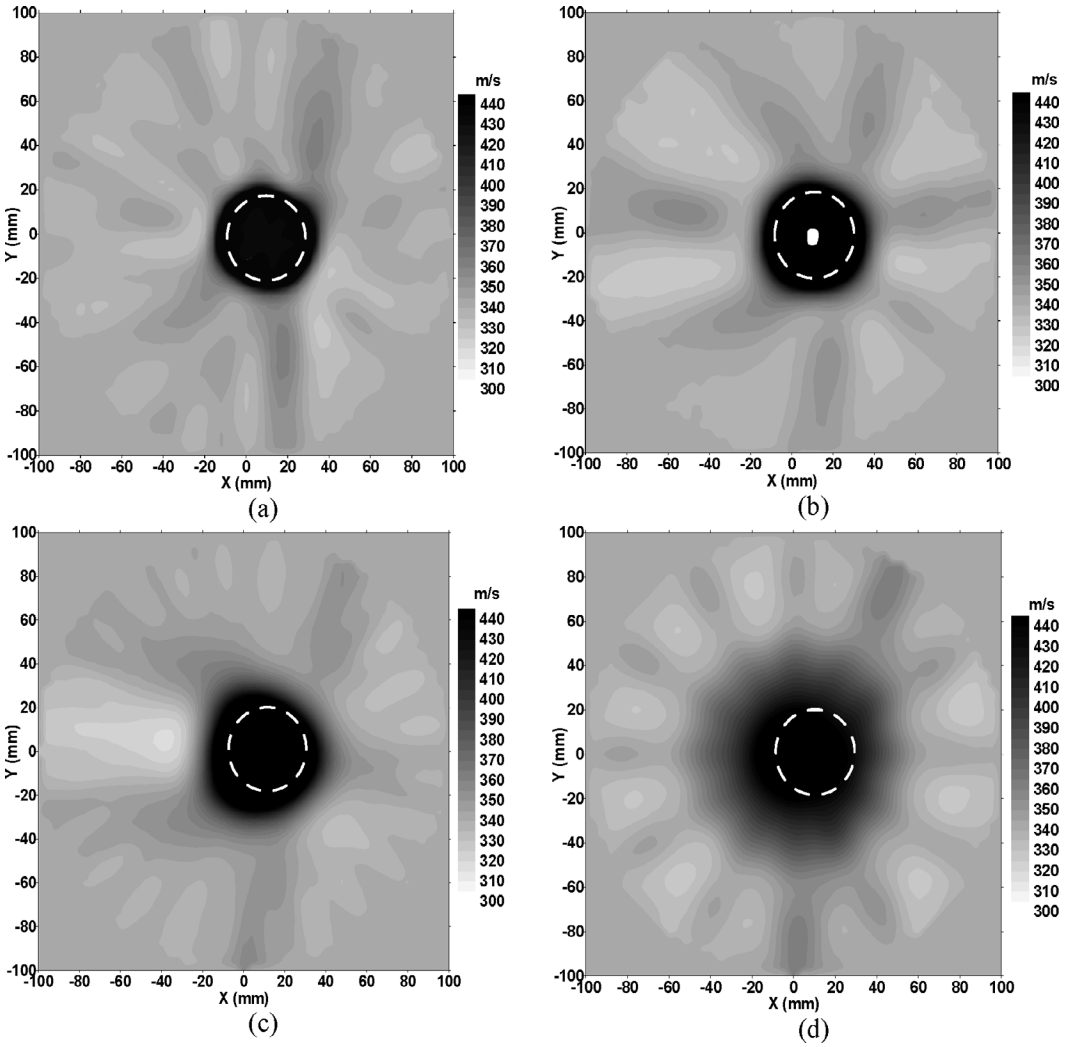

Fig. 9. Images of a 38-mm diameter solid aluminium cylinder in air with its center at (10,0), reconstructed using the Hamming filter. (a) 2664 rays, (b) 684 rays, (c) 312 rays, and (d) 84 rays. The dashed white circle shows the true size and location of the cylinder.

curs to the signal passing through the scan area, which would affect the accuracy of the reproduced temperature. The data collection took several hours, which means the overall scan also would be time averaged over this period. Scans using the thermocouple were more rapid, giving a more accurate temperature profile. Room temperature was not constant; and, as this form of tomography used a difference technique based on the first ray of the first projection, any variations in ambient temperature after this initial data was acquired would directly affect the reproduced temperature within the scan area. There were no environmental controls such as air conditioning or heating in the laboratory, and personnel access was restricted during each scan. On comparison of the propagation delays and speeds of sound calculated using the very first ray and very last ray of the entire scan shown, the overall change in room temperature during the data acquisition was only 3 K.

It is clear from Fig. 6(a) that the area of increased temperature has a diameter of approximately 40 mm (equating to a minimum sampling rate of approximately 50 samples/m). As was the case with the object imaging, the reconstruction in Fig. 6(b) again gives an accurate temperature reconstruction of 337 K when only one quarter of the original data is used. Figs. 6(c) and (d) reconstruct center temperatures of 326 K and 315 K, respectively, which equate to accuracies of 94.8% and 91.6%, respectively. This drop off in accuracy again can be attributed to aliasing effects resulting from sampling rates below 50 samples/m. It is interesting to note that, in the under-sampled temperature images shown in Figs. 6(c) and (d), there are no obvious aliasing defects. Thus, if the expected size and temperature of the affected region is unknown, there are few clues in an image that under-sampling has occurred. In this event, the reconstructed values of temperature will be significantly less than the actual values.

C. Changing the Kernel Filter Function

The standard Ram-Lak filter was modified with a Hamming, cosine or Shepp-Logan window, as shown in Fig. 7, and the effects of these different window functions on the

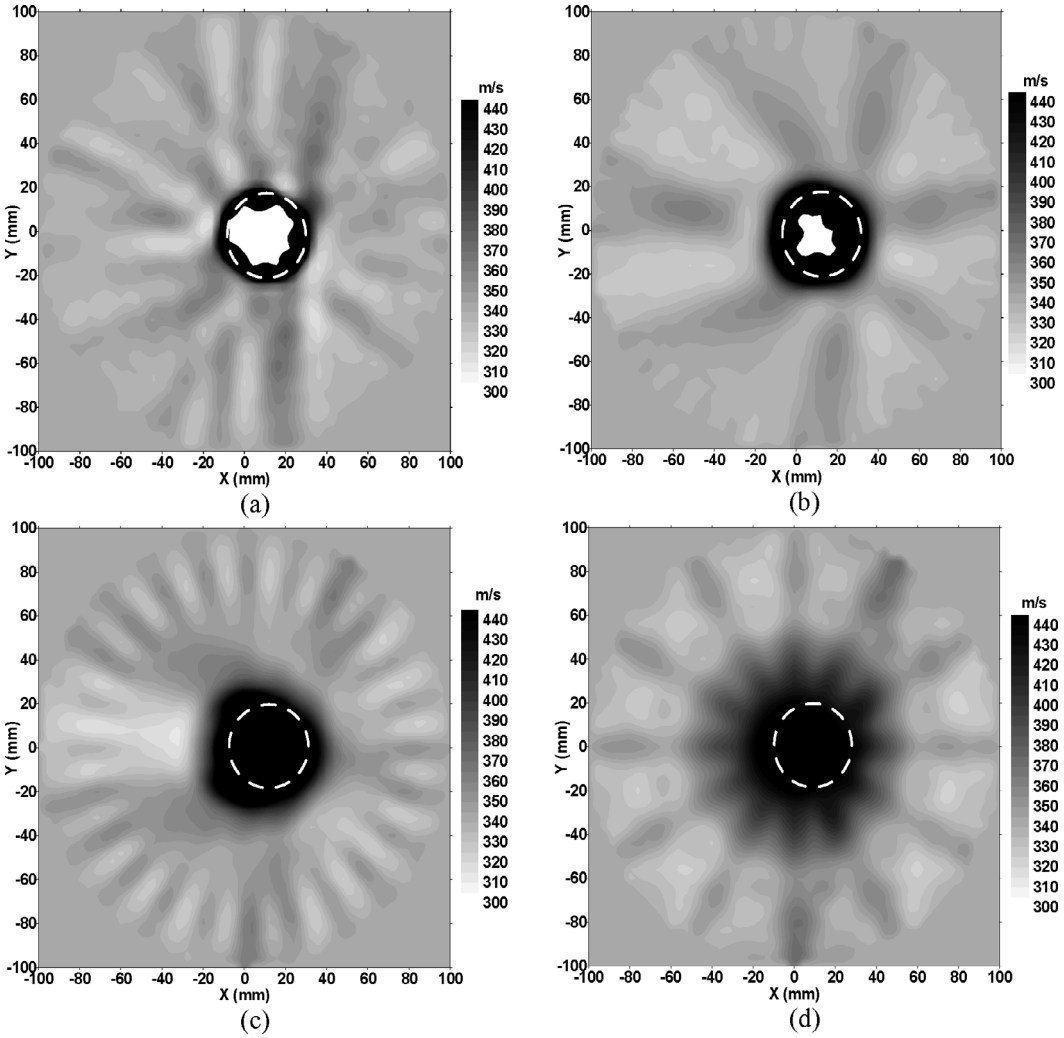

Fig. 10. Images of a 38-mm diameter solid aluminium cylinder in air with its center at (10,0), reconstructed using the Shepp-Logan filter. (a) 2664 rays, (b) 684 rays, (c) 312 rays, and (d) 84 rays. The dashed white circle shows the true size and location of the cylinder.

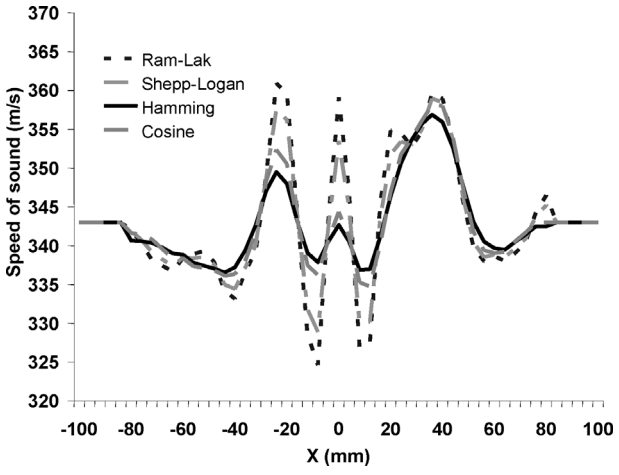

Fig. 11. A comparison of sections at $Y = 60$ mm through Figs. 5(a), 8(a), 9(a), and 10(a) to indicate the effects of the Ram-Lak, cosine, Hamming, and Shepp-Logan filters. The ends of each plot correspond to corner regions of the reconstructed image that contain no measured data values.

reconstructed images were studied. All the window functions are used primarily to reduce the sharp step at the end of the Ram-Lak function and reduce the noise this introduces into the reconstructed images. Unfortunately, the window functions also reduce the effective bandwidth of the data. Figs. 8(a) to (d) show the same solid cylinder of Fig. 6, but reconstructed with a cosine window applied to the basic Ram-Lak function. As can be seen, the high-frequency noise has been reduced, as has the appearance of the aliasing artefacts. But the apparent size of the bar has increased slightly due to blurring of the edges. Figs. 9(a) to (d) show the results obtained using a Hamming window. The noise and appearance of the artefacts have been reduced further. Note also that the reconstructed values within the solid cylinder also have decreased. This is to be expected, as the cosine and Hamming window functions emphasize the mid-range of spatial frequencies and reduce the effects of high-frequency noise. Compare these plots with those of Figs. 10(a) to (d), which use a Shepp-Logan window. There has been only a marginal reduction in noise from using the Ram-Lak function, as the Shepp-

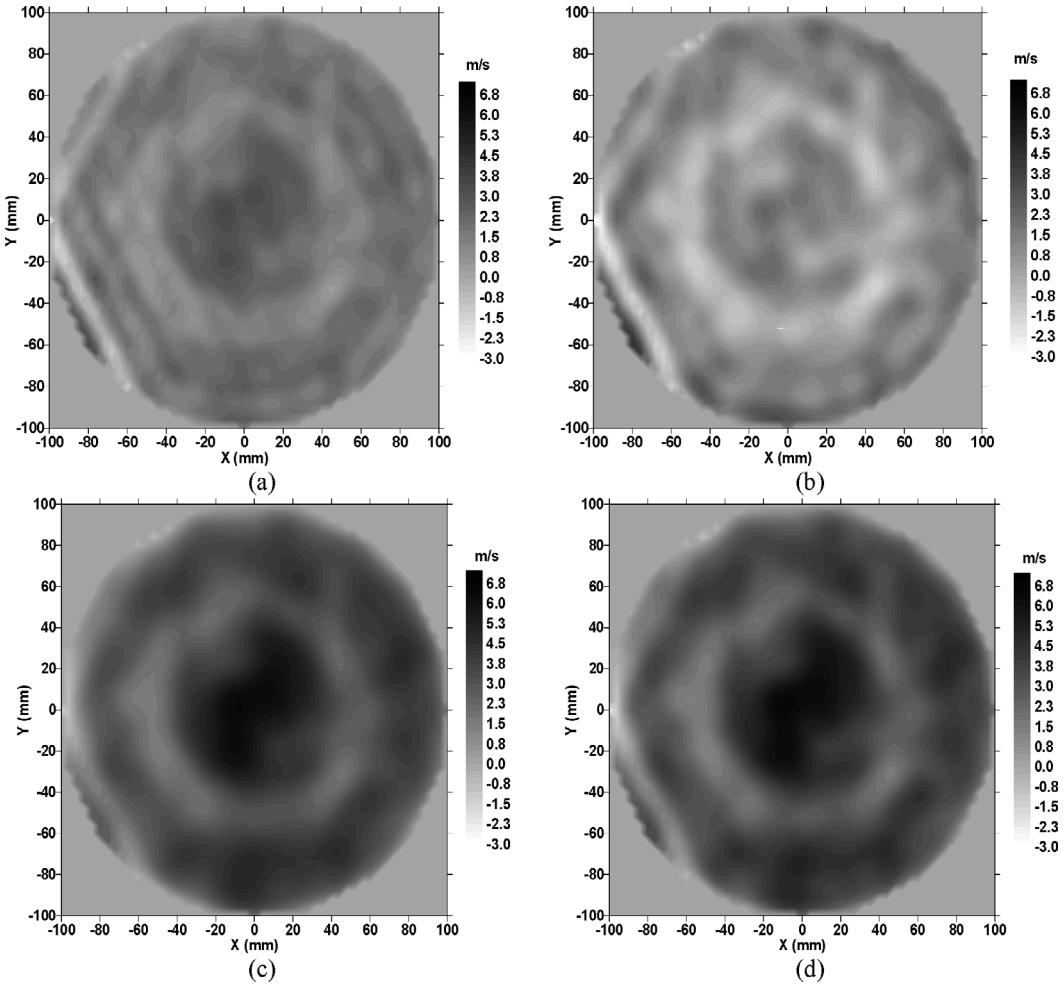

Fig. 12. Reconstructed image of air flow above a nozzle using 2664 rays. a) The Ram-Lak filter, (b) the Shepp-Logan filter, (c) the Hamming filter, and (d) the cosine filter.

Logan function tends to emphasize the higher frequencies and suppress the lower frequencies. Fig. 11 shows a comparison of sections through the center of each image in Fig. 10 at Y = 60 mm to aid in the interpretation of filter effects. In each case, the different windowing functions reduce the magnitude of the reconstructed values as well as the noise content of the basic Ram-Lak data, with the Shepp-Logan function producing only a mild smoothing effect, and the Hamming window producing the largest change. This is to be expected on comparing the relative spectral content of each function in Fig. 7.

D. Reconstruction of Flow Fields

Fig. 12(a) to (d) shows the reconstructed images of the flow profile above a 2.7 mm diameter nozzle connected to a compressed air source with a flow rate of 0.5 l/s measured using a variable area A10HS flowmeter (Platon Instrumentation, Basingstoke, UK). These figures show the additional horizontal components of the flow velocity of the air jet, reconstructed from slowness data using a background speed of sound of 347 m/s. The jet is expanding radially outward from the center, hence outward flow components will be seen as an increase in velocity, and inward components will be seen as a decrease. As the turbulent flow from the nozzle is rapidly fluctuating, the velocities are effectively time averaged over the data acquisition period and the values reconstructed within the scan area are affected by other constraints concerning the size of the transducers leading to spatially averaged values, compressibility of the air, and ray bending. Note also the bad rays in the left of each image. Despite these limitations, the maximum horizontal flow component is shown to be up 7.0 m/s at the center of the scan area, which is in good agreement with theory as demonstrated in earlier work using parallel beams [25]. The images in Fig. 12 show the effects of the different filter functions for a dataset of 2664 rays, as the images produced by using reduced datasets produced similar effects to those for the temperature images in Fig. 6—the reconstructed values were lower and the affected region was enlarged. The optimum choice of filter window function and interpretation of the images in this instance is rather subjective, as the flow magnitude and the size of the affected area in the scanning plane produced by the spreading air jet cannot be precisely determined. Fig. 13 shows a comparison of sections through the center of each

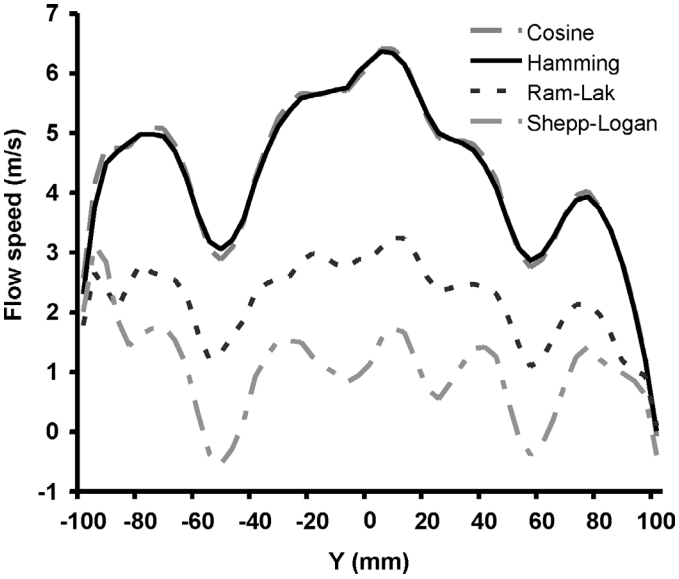

Fig. 13. A comparison of sections at $X = 0$ mm through Figs. 12(a) to (c) to compare the effects of the Ram-Lak, cosine, Hamming, and Shepp-Logan filters on the reconstruction of air flow.

image in Fig. 12 at X = 0 mm to help visualize the effects of each filter. The Shepp-Logan filter produces lower values in the reconstruction than when using the basic Ram-Lak, whereas the cosine and Hamming functions produce higher reconstructed values from the same data. Referring back to Fig. 7, it can be seen that the Shepp-Logan filter reduces the effects of normalized frequency components up to 0.2 when compared with the cosine and Hamming filters, implying that these frequencies are important in the formation of the images shown in Fig. 12. Hence, it is uncertain as to whether the Hamming or cosine filters in Figs. 12(c) and (d) that appear to smooth the reconstructed images give more realistic results. However, for faster acquisition times, more of the turbulent detail could be included in the image, and the Ram-Lak or Shepp-Logan filter used in Figs. 12(a) and (b) then may be more appropriate.

V. Conclusions

A fan-beam, air-coupled, through-transmission tomographic imaging system has been developed along with an occluded data compensation algorithm that not only locates highly reflective objects within the scanning plane, but also allows the simultaneous reconstruction of the spatial variations in speed of sound in the surrounding air. These changes in speed of sound also can be used to produce images of spatial variations in temperature and air flow. The system produced an equivalent level of reconstruction accuracy as a previous parallel beam system, but used a more efficient fan-beam method of data acquisition. The effects of aliasing artefacts were investigated by reducing the size of the datasets used in the reconstruction. Although Gibbs' phenomena could be seen in the images of solid objects, such artefacts were not apparent in reconstructions of temperature or flow, and the reconstructed values were lower and the affected areas appeared larger. By selection of the appropriate window function in the reconstruction process, the images could be optimized in terms of noise and feature enhancement.

References

[1] J. Greenleaf, S. Johnson, W. Wamoya, and F. Duck, "Algebraic reconstruction of spatial distributions of acoustic velocities in tissue from their time-of-flight profiles," *Acoust. Hologr.*, vol. 6, pp. 71–90, 1975.

[2] I. L. Meglis, T. Chow, C. D. Martin, and R. P. Young, "Assessing in situ microcrack damage using ultrasonic velocity tomography," *Int. J. Rock Mech. Mining Sci.*, vol. 42, pp. 25–34, 2005.

[3] A. C. Kak and M. Slaney, *Principles of Computerized Tomographic Imaging*. New York: IEEE Press, 1988.

[4] L. Capineri, H. G. Tattersall, J. A. G. Temple, and M. G. Silk, "Time-of-flight diffraction tomography for NDT applications," *Ultrasonics*, vol. 30, no. 5, pp. 275–288, 1992.

[5] K. A. Dines and S. A. Goss, "Computed ultrasonic reflection tomography," *IEEE Trans. Ultrason., Ferroelect., Freq. Contr.*, vol. 34, no. 3, pp. 309–318, 1987.

[6] A. J. Devaney, "Fast filtered backpropagation algorithm for ultrasound tomography," *IEEE Trans. Ultrason., Ferroelect., Freq. Contr.*, vol. 34, pp. 330–340, 1987.

[7] R. M. Lewitt, "Reconstruction algorithms: Transform methods," *Proc. IEEE*, vol. 71, pp. 390–408, 1984.

[8] R. Gordon, R. Bender, and G. T. Hermann, "Algebraic reconstruction techniques for three-dimensional electron microscopy and X-ray photography," *J. Theor. Biol.*, vol. 29, pp. 471–481, 1970.

[9] Y. Censor, "Finite series-expansion reconstruction techniques," *Proc. IEEE*, vol. 71, pp. 409–419, 1984.

[10] L. J. Xu and L. A. Xu, "Gas/liquid two-phase flow regime identification by ultrasonic tomography," *Flow Meas. Instrum.*, vol. 8, pp. 145–155, 1998.

[11] O. M. Warsito, N. Kawata, and S. Uchida, "Cross-sectional distributions of gas and solid holdups in slurry bubble column investigated by ultrasonic computed tomography," *Chem. Eng. Sci.*, vol. 54, no. 21, pp. 4711–4728, 1999.

[12] V. Bucur, "Ultrasonic techniques for nondestructive testing of standing trees," *Ultrasonics*, vol. 43, pp. 237–239, 2005.

[13] A. M. H. Satti and J. Szilard, "Computerized ultrasonic tomography for testing solid propellant rocket motors," *Ultrasonics*, vol. 21, pp. 162–166, 1983.

[14] W. M. D. Wright, D. A. Hutchins, D. P. Jansen, and D. W. Schindel, "Air-coupled Lamb wave tomography," *IEEE Trans. Ultrason., Ferroelect., Freq. Contr.*, vol. 44, pp. 53–59, 1997.

[15] E. V. Malyarenko and M. K. Hinders, "Ultrasonic Lamb wave diffraction tomography," *Ultrasonics*, vol. 39, pp. 269–281, 2001.

[16] H. Carr and C. Wykes, "Diagnostic measurements in capacitive transducers," *Ultrasonics*, vol. 31, pp. 13–20, 1993.

[17] M. Oksanen, J. Varis, J. Hietanen, and J. Wu, "Quantitative theory for V-groove capacitive transmitting transducers," *Ultrasonics*, vol. 35, pp. 205–211, 1997.

[18] A. S. Fiorillo, "PVDF ultrasonic sensors for location of small objects," *Sens. Actuators A: Physi.*, vol. 42, pp. 406–409, 1994.

[19] R. L. O'Leary and G. Hayward, "Investigation into the effects of modification of the passive phase for improved manufacture of 1-3 connectivity piezocomposite transducers," *IEEE Trans. Ultrason., Ferroelect., Freq. Contr.*, vol. 46, pp. 511–516, 1999.

[20] B. Khuri-Yakub, F. Degertekin, X. Jin, S. Calmes, I. Ladabaum, S. Hansen, and X. Zhang, "Silicon micromachined ultrasonic transducers," in *Proc. IEEE Ultrason. Symp.*, 1998, pp. 985–991.

[21] D. Schindel, D. Hutchins, L. Zou, and M. Sayer, "The design and characterization of micromachined air-coupled capacitance transducers," *IEEE Trans. Ultrason., Ferroelect., Freq. Contr.*, vol. 42, pp. 42–50, 1995.

[22] G. Caliano, F. Galanello, A. Caronti, R. Carotenuto, and M. Pappalardo, "Micromachined ultrasonic transducers using sil-

icon nitride membrane fabricated in PECVD technology," in *Proc. IEEE Ultrason. Symp.*, 2000, pp. 963–967.
[23] P. C. Eccardt, K. Niederer, T. Scheiter, and C. Hierold, "Surface micromachined ultrasound transducers in CMOS technology," in *Proc. IEEE Ultrason. Symp.*, 1996, pp. 959–962.
[24] G. J. Brown and D. Reilly, "Ultrasonic tomographic imaging of solid objects in air using an array of fan-shaped-beam electrostatic transducers," *Ultrasonics*, vol. 34, pp. 111–115, 1996.
[25] W. M. Wright, D. W. Schindel, D. A. Hutchins, P. W. Carpenter, and D. P. Jansen, "Ultrasonic tomographic imaging of temperature and flow fields in gases using air-coupled capacitance transducers," *J. Acoust. Soc. Amer.*, vol. 104, pp. 3446–3455, 1998.
[26] T. H. Gan, D. A. Hutchins, P. W. Carpenter, and D. R. Billson, "Simultaneous reconstruction of flow and temperature cross-sections in gas jets using air-coupled ultrasonic tomography," in *Proc. IEEE Ultrason. Symp.*, 2001, pp. 623–626.
[27] T. H. Gan and D. A. Hutchins, "Air-coupled ultrasonic tomographic imaging of high-temperature flames," *IEEE Trans. Ultrason., Ferroelect., Freq. Contr.*, vol. 50, pp. 1214–1218, 2003.
[28] T. M. Peters and R. M. Lewitt, "Computed tomography with fan-beam geometry," *J. Comput. Assist. Tomog.*, vol. 1, pp. 429–436, 1977.
[29] P. Ingleby and W. M. D. Wright, "Ultrasonic imaging in air using fan-beam tomography and electrostatic transducers," *Ultrasonics*, vol. 40, pp. 507–511, 2002.
[30] R. Hickling and S. P. Marin, "The use of ultrasound for gauging and proximity sensing in air," *J. Acoust. Soc. Amer.*, vol. 79, pp. 1151–1160, 1986.

William M. D. Wright (M'98) received his B.Eng. and Ph.D. degrees in engineering from the University of Warwick, England in 1991 and 1996, respectively. He continued to work there as a Postdoctoral Research Fellow until 1997 when he joined University College Cork, Ireland as a lecturer in the Department of Electrical and Electronic Engineering. His research interests include non-contact ultrasound, tomographic imaging, and transducer development.

Paul Ingleby received his Ph.D. degree in Engineering from the University of Warwick, UK in 1998 for his research into Polymer Gas Sensors. He expanded his research interest to non-contact ultrasonic sensors through continued post-doctoral research at Warwick and subsequently through a Marie Curie Research Fellowship at University College Cork, Ireland. He now works as a Principal Systems Engineer at SELEX Sensors and Airborne Systems Ltd, UK.

Ian J. O'Sullivan received his B.Eng. degree in Chemical Engineering from Cork Institute of Technology in 1996, and his M.Eng.Sc. degree in Food Engineering from University College Cork in 1999. He is currently pursuing a Ph.D. degree in University College Cork, where his research interests include tomographic imaging and ultrasonic flow measurement.